

# Testbeam and laboratory test results of irradiated 3D CMS pixel detectors

Mayur Bubna<sup>a,k</sup>, Enver Alagoz<sup>a</sup>, Alex Krzywda<sup>a</sup>, Mayra Cervantes<sup>a</sup>, Kirk Arndt<sup>a</sup>, Margherita Obertino<sup>b</sup>, Ada Solano<sup>b</sup>, Gian-Franco Dalla Betta<sup>i</sup>, Marco Povoli<sup>i</sup>, Mario Denace<sup>c</sup>, Luigi Moroni<sup>c</sup>, Jennifer Ngadiuba<sup>c</sup>, Stefano Terzo<sup>c</sup>, Simon Kwan<sup>d</sup>, Ryan Rivera<sup>d</sup>, Lorenzo Uplegger<sup>d</sup>, Alan Prosser<sup>d</sup>, Ilya Osipenkov<sup>g</sup>, CM Lei<sup>d</sup>, Ping Tan<sup>d</sup>, Jeff Andresen<sup>d</sup>, Nhan Tran<sup>d</sup>, John Chramowicz<sup>d</sup>, Daniela Bortoletto<sup>a</sup>, Gino Bolla<sup>a</sup>, Ian Shipsey<sup>a</sup>, Marco Boscardin<sup>j</sup>, John Cumalat<sup>e</sup>, Frank Jensen<sup>e</sup>, Stephen R. Wagner<sup>e</sup>, Ashish Kumar<sup>f</sup>, Richard Brosius<sup>f</sup>, Lalith Perera<sup>h</sup>

<sup>a</sup>Purdue University, Department of Physics, West Lafayette, IN 47907-1396, USA

<sup>b</sup>Istituto Nazionale di Fisica Nucleare, Sezione di Torino, 10125 TORINO, Italy

<sup>c</sup>Istituto Nazionale di Fisica Nucleare, Sezione di Milano Bicocca, and Università degli Studi di Milano Bicocca, 20126 Milano, Italy

<sup>d</sup>Fermi National Accelerator Laboratory, Batavia, IL 60510-0500, USA

<sup>e</sup>University of Colorado at Boulder, Department of Physics, Boulder, CO 80309-0390, USA

<sup>f</sup>State University of New York at Buffalo (SUNY), Department of Physics, Buffalo, NY 14260-1500, USA

<sup>g</sup>Texas A&M University, Department of Physics, College Station, TX 77843-4242, USA

<sup>h</sup>University of Mississippi, Department of Physics and Astronomy, University, MS 38677, USA

<sup>i</sup>INFN Padova (Gruppo Collegato di Trento) and Dipartimento di Ingegneria e Scienza dell'Informazione, Università di Trento, I-38123 Povo di Trento (TN), Italy

<sup>j</sup>Centro per i Materiali e i Microsistemi Fondazione Bruno Kessler (FBK), Trento, I-38123 Povo di Trento (TN), Italy

<sup>k</sup>Purdue University, School of Electrical and Computer Engineering, West Lafayette, IN 47907-1396, USA

---

## Abstract

The CMS silicon pixel detector is the tracking device closest to the LHC p-p collisions, which reconstructs precisely the charged particle trajectories. The planar technology used in the current innermost layer of the pixel detector has reached the design limit for radiation hardness. As a possible replacement of planar technology for the High Luminosity-LHC or HL-LHC, 3D silicon technology is under consideration due to its unprecedented good performance in harsh radiation environments. 3D silicon detectors are fabricated by the Deep Reactive-Ion-Etching (DRIE) technique which allows p- and n-type electrodes to be processed through the silicon substrate as opposed to being implanted on silicon surface. The 3D CMS pixel devices presented in this paper were processed at FBK. They were bump bonded to the current CMS pixel readout chip, tested in the laboratory, and testbeams carried out at FNAL with the proton beam of 120 GeV/c. In this paper we present the laboratory and beam test results for the irradiated 3D CMS pixel devices.

**Keywords:** CMS pixel detector, LHC upgrade, 3D technology, radiation hardness

---

## 1. Introduction

The innermost CMS pixel tracker detector [1] will undergo an upgrade in preparation for the so called High Luminosity LHC or HL-LHC, which will provide ten times higher particle collisions in 2020 [2]. The CMS pixel detector will be exposed to a fluence of  $10^{16}$  n<sub>eq</sub>/cm<sup>2</sup>, which is ten times higher than the design fluence for the current detector, during the operation of HL-LHC [3]. Furthermore, current CMS pixel sensors have already shown serious performance degradation at the fluence of  $10^{15}$  n<sub>eq</sub>/cm<sup>2</sup> [4], demonstrating that they will not withstand higher radiation doses. One of the top candidates for replacing the current planar technology is three dimensional silicon technology [5]. 3D silicon detectors are fabricated by the Deep Reactive-Ion-Etching (DRIE) technique, which allows p- and n-type electrodes to be processed through the silicon substrate, as opposed to being implanted on silicon surface. Therefore, the charge carrier collection distance is decoupled from the thickness of the silicon substrate. This feature makes 3D sensors; radiation hard due to short inter-electrode distance that provides faster charge collection without being trapped by radiation in-

duced damage in silicon; have lower depletion voltages compared to the planar sensors. The drawbacks of this technology are high sensor capacitance and complex fabrication processing. ATLAS IBL collaboration decided to use 3D pixel detectors for the forward part of IBL [6], and studies are in progress for using 3Ds in near proton spectrometers at LHC [7].

In order to reduce the cost and improve yield, Fondazione Bruno Kessler (FBK), Trento, Italy [8], and Centro Nacional de Microelectronica (CNM-IMB), Barcelona, Spain [9], have independently developed the so-called 3D Double-side Double-Type Column (3D-DDTC) sensors. Double-sided 3D sensors indeed offer some advantages in terms of process complexity with respect to the original Full 3D sensor technology. In particular, there is no need for oxide bonding and removing a support wafer, which reduces the number of process steps and makes the backside of the wafer fully accessible to apply substrate bias. A disadvantage of double-sided detectors is that they do not have an active edge, but by using a properly designed termination the dead area at the edge can be reduced to about 100  $\mu$ m [16]. The 3D collaboration has been extended to include SINTEF (Norway) [13], which is committed to small to medium

scale production of active edge full-3D silicon sensors. The intrinsic feature of the SINTEF 3D detector is that it can be fabricated with an active edge so that the width of the dead periphery can be reduced to only a few microns. 3D detectors also surpass the planar ones in terms of low charge sharing.

The sensors considered in this study are 3D pixel sensors from FBK Double-side Double-type Column (3D-DDTC) ATLAS08 batch and 3D 1E diodes from FBK ATLAS10 batch. The CMS 1E 3D diodes from ATLAS10 batch have a p-type material of thickness  $200\ \mu\text{m}$  and consists of a  $19 \times 29$  pixel array. These devices reproduce the same column configurations and geometries of their parent pixel sensors, but have all columnar electrodes of the same doping type shorted together with a metal grid or a combination of metal grid and surface implantations. This creates a device with only two terminals which eases the testing without the need of complex bonding solutions [15]. The 3D pixel sensors are from ATLAS08 batch with a p-type material of thickness  $200 \pm 20\ \mu\text{m}$  and consists of a  $52 \times 80$  pixel array. The sensors have different electrode configurations (1E, 2E and 4E) and were bump-bonded to the CMS PSI46v2 Read-out Chip.

The sensors from ATLAS08 were irradiated at the Los Alamos LANCSE facility with 800 MeV protons to  $7 \times 10^{14}\ \text{n}_{\text{eq}}/\text{cm}^2$  and  $3.5 \times 10^{15}\ \text{n}_{\text{eq}}/\text{cm}^2$  fluences. Also, the 3D diodes from ATLAS10 were irradiated with  $\text{Co}^{60}$  gamma source to a dose of 2.3 Mrad. The 3D diodes were actively biased during irradiation. This was done to understand the breakdown performance of the new fabrication technology in ATLAS10 batch.

## 2. Electrical characterization

FBK 3D sensors were characterized in the laboratory at room temperature. The measured leakage currents as a function of the bias voltage are shown in Figure 1 for candidate 1E and 2E devices. After bump bonding, the typical leakage currents are less than 150 nA for 1E and about  $10\ \mu\text{A}$  for 2E devices. The breakdown voltage is between 20 V and 40 V. The devices were found to be fully depleted around 10 V, so there is no effect of lower breakdown voltage on charge collection efficiency. Figure 1 also shows the leakage current measured at  $-20^\circ\text{C}$  after  $7 \times 10^{14}\ \text{n}_{\text{eq}}/\text{cm}^2$  proton irradiation. After irradiation, the leakage current increases to  $\sim 1\ \mu\text{A}$  while there is not much improvement in the breakdown voltage.

The ATLAS08 batch in particular experienced problems during the fabrication process, which have been fixed in the more recent batches like ATLAS10. The lower breakdown voltage in ATLAS08 was probably caused by higher p-spray doping in the devices [14]. The p-spray doping was reduced in ATLAS10 batch which improved the breakdown voltage behavior. There are a few devices with much higher leakage current and early breakdown in ATLAS08 batch which are likely caused by fabrication induced defects inside the sensors. Figure 2 shows the leakage current measurements of 3D 1E diodes from ATLAS10 batch before and after  $\text{Co}^{60}$  gamma irradiation. The leakage current was  $\sim 10\ \text{nA}$  for the diodes before irradiation which improved a little after irradiation. There was a tremendous improvement in breakdown from 40 V to 80 V. Since

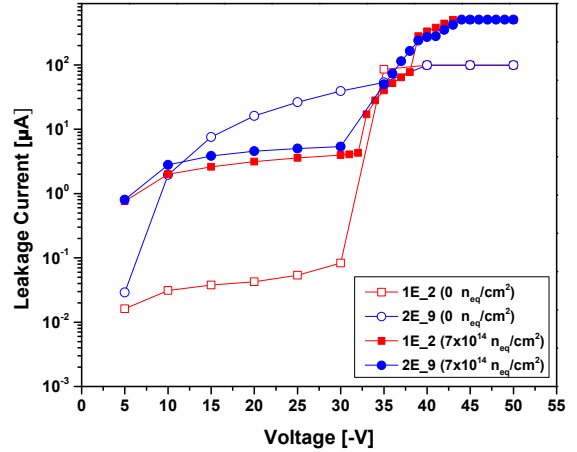


Figure 1: IV curve of 3D pixel sensors before irradiation at  $20^\circ\text{C}$  and after  $7 \times 10^{14}\ \text{n}_{\text{eq}}/\text{cm}^2$  proton irradiation at  $-20^\circ\text{C}$ .

gamma irradiation mostly affects the surface behavior of the devices, the improvement in breakdown voltage may be related to improved interface carrier concentration and better surface mobility which leads to improved leakage current and higher breakdown voltage.

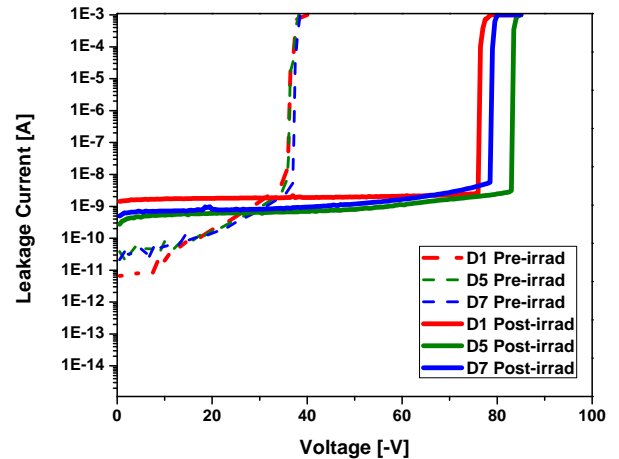


Figure 2: IV curve of 3D 1E diodes before irradiation at  $20^\circ\text{C}$  and after 2.2 Mrad  $\text{Co}^{60}$  gamma irradiation at  $-20^\circ\text{C}$  with the devices actively biased at  $-10\ \text{V}$ .

## 3. I-T measurements

Current-temperature ( $I$ - $T$ ) measurements can be used to extract information about the different mechanisms responsible for the leakage current generation in reverse biased diodes. When diode is biased to be in full depletion but below the breakdown voltage ' $V_{\text{BD}}$ ' of the device, the leakage current generation is expected to be dominated by Shockley-Reed-Hall (SRH) mechanism. As the applied bias approaches  $V_{\text{BD}}$ , impact ionization starts and the effect of temperature dependence on leakage current generation becomes weaker. We measured  $I$ - $T$  behavior for several 3D diodes from ATLAS10 batch by biasing them above depletion voltage but well below the breakdown

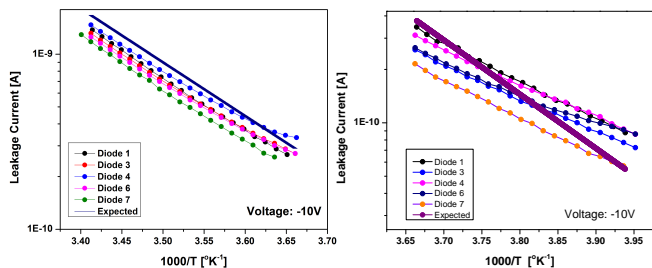


Figure 3: Comparison between measured (dotted) and calculated (solid) values of leakage current before irradiation at a bias voltage of -10 V from (a) 0°C to 20°C and (b) 0°C to -20°C.

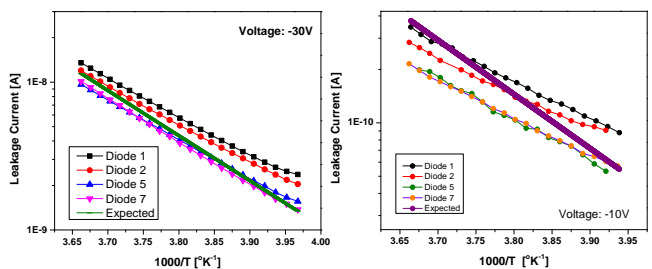


Figure 4: Comparison between measured (dotted) and calculated (solid) values of leakage current from (a) 0°C to -20°C at -30 V after irradiation and (b) before irradiation at -10 V from 0°C to -20°C.

voltage of these devices: -10 V for diodes before irradiation and -30 V for irradiated diodes. Under these conditions, SRH generation is expected to be the driving leakage mechanism in which case the current must be proportional to the intrinsic carrier concentration  $n_i$  which implies that current is proportional to temperature as  $I \sim n_i \sim T^2 e^{-(E_g/2k_B T)}$  [17]. Figure 3 gives the  $I$ - $T$  dependence in a semi-log plot for 3D diodes from 20°C to 0°C and from 0°C to -20°C. Figure 3 (left) shows that the agreement between measured and expected temperature dependence is good only at high temperatures. At low temperatures (0°C to -20°C), Figure 3 (right) shows that the leakage currents does not exhibit a pure SRH type behavior; in fact the temperature dependence gets weaker.

The 3D diodes were irradiated with  $\text{Co}^{60}$  gamma irradiator to a dose of 2.3 Mrad. Figure 4 (left) shows the  $I$ - $T$  measurements performed on the diodes from 0°C to -20°C. Figure 4 (right) shows the results of  $I$ - $T$  measurement before irradiation for comparison. After irradiation, the slopes of  $I$ - $T$  curves appear parallel to the slope of intrinsic carrier concentration  $n_i$  indicating the leakage current generation after irradiation is dominated by SRH generation and any other generation mechanisms have been relatively suppressed.

#### 4. Laboratory and testbeam measurements

Sensors were tested with a  $\text{Sr}^{90}$  radioactive source for lab measurements and also with 120 GeV/c protons at the Fermilab Meson Test Facility. The Fermilab testbeam setup is described in [10]. The telescope made of eight planes of planar CMS FPIX pixel detectors was used to reconstruct the tracks. The intrinsic track resolution is about 7  $\mu\text{m}$  in both the X and Y local

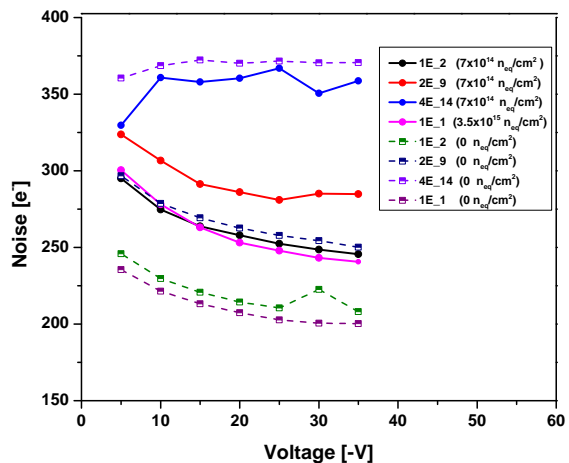


Figure 5: Noise of FBK 3D sensors from ATLAS08 measured before irradiation at 20°C and after  $7 \times 10^{14} \text{ n}_{\text{eq}}/\text{cm}^2$  fluence at -20°C.

coordinates. The trigger signal is provided by two PMTs coupled to scintillators downstream from the telescope. No magnetic field is applied. DUTs are tilted to various angles with respect to the beam to improve resolution. Event data from the test beam is analyzed using software developed specifically for the Fermilab test beam.

The S-curve test was used to determine the pixel noise by sending internal calibration signals through the injection capacitor to the ROC preamplifier input and measuring the response efficiency on a pixel-by-pixel basis. Noise measurements are taken at room temperature before irradiation, and at -20°C after irradiation. The tests are based on single measurements with no averaging of S-curve results. Figure 5 shows the noise results measured before and after irradiation. Capacitance (and thus noise) increases with radiation damage or smaller electrode spacing, but decreases with reverse bias. All of these behaviors are clearly seen in the 1E and 2E sensors. Noise increases by 20-30% in the 1E sensors and around 10% in the 2E sensors. The mean value of the noise distribution measured at full depletion for the 2E detectors considered in this study is  $\sim 250 \text{ e}^-$  before irradiation at 20°C and it increases to  $\sim 290 \text{ e}^-$  at -20°C after  $7 \times 10^{14} \text{ n}_{\text{eq}}/\text{cm}^2$  fluence.

Figure 6 shows the charge collected with a  $\text{Sr}^{90}$  source before and after irradiation. Random trigger was used to collect data. The sensors were biased at -30 V and a threshold of 3900 electrons was used. The collected charge before irradiation varied between 12  $\text{ke}^-$  and 14  $\text{ke}^-$ . There is a signal loss of 43% after  $7 \times 10^{14} \text{ n}_{\text{eq}}/\text{cm}^2$  in 1E, 50% after  $3.5 \times 10^{15} \text{ n}_{\text{eq}}/\text{cm}^2$  in 1E, 14% after  $7 \times 10^{14} \text{ p}/\text{cm}^2$  in 2E, and 14% after  $7 \times 10^{14} \text{ p}/\text{cm}^2$  in 4E sensors. For comparison, the signal loss in CMS planar pixels is about 50% after  $1 \times 10^{15} \text{ n}_{\text{eq}}/\text{cm}^2$  at 600V. The collected charge is what is expected in thick silicon (16  $\text{ke}^-$ ) only if the track hits the central part of the pixel; elsewhere it is reduced by the combined effect of charge sharing and readout chip threshold.

Figure 7 shows the cell efficiency for an individual 2E pixel before and after irradiation obtained from testbeam measurements. An event's efficiency is equal to one if a hit is regis-

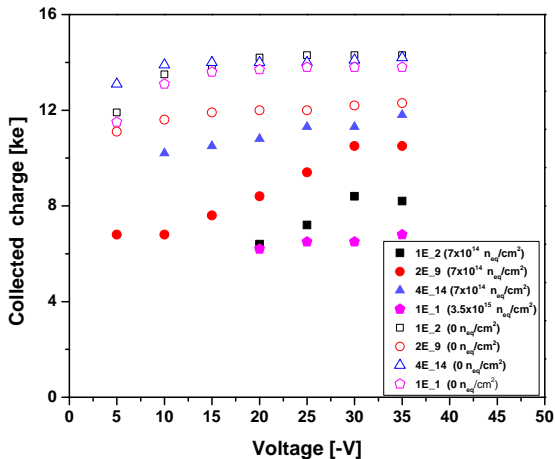


Figure 6: Charge collected for FBK 3D sensors from ATLAS08 measured before irradiation at 20°C and after  $7 \times 10^{14}$   $n_{eq}/cm^2$  proton irradiation at -20°C.

tered within one pixel width of a reconstructed track and zero otherwise. Efficiency is studied at normal beam incidence to the sensor plane. Only events with one track are considered. The total sensor efficiency is determined by averaging the efficiency of all the events in a run. Efficiency increases with bias due to larger electric fields in the bulk, up to breakdown voltage after which it falls off. Radiation level has a significant effect on efficiency far away from the readout. The efficiency was measured at different bias voltages and at different angles. For all devices, it increases with bias voltage and saturates at -20 V, where sensors are completely depleted. Figure 7 (left) shows the efficiency of a single pixel before irradiation reconstructed from all the track information. The sensor was biased at -5 V with the detector orthogonal to the beam (angle of 0°). The efficiency increases by rotating the DUT with respect to the beam axis, reaching a value of ~95.4% before irradiation. The small decrease in full efficiency is partially explained by the electrodes being inactive volumes for tracks impinging orthogonal to the detector. This is shown in Figure 7 (left) where structures corresponding to the n+ columns in the middle of the sensor and to the six p+ columns on the edges are visible. After irradiation the fluence of  $7 \times 10^{14}$   $n_{eq}/cm^2$ , the efficiency of the sensor reduced to 91.1% as shown in Figure 7 (right).

Track residuals are calculated as the distance between the predicted and measured positions of a cluster, in either the local X or Y direction. The residuals are fitted with a Gaussian; the overall sensor resolution is determined from the sigma of the fit. Best post-irradiation residual obtained for a 2E sensor was  $12.56 \mu m$ .

## 5. Conclusions and Outlook

3D sensors offer several improvements over planar sensors, especially at higher luminosities but suffer from higher noise compared to planar sensors. The breakdown voltage of sensors received from FBK increased after improvements in fabrication processing and better control over p-spray doping. Pre-irradiation beam test results show efficiencies higher than 90%

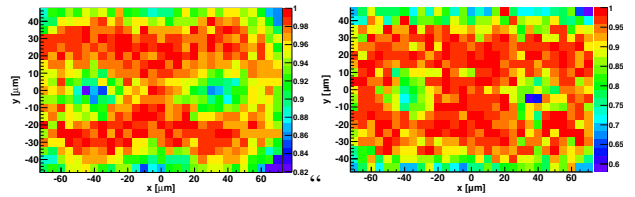


Figure 7: Cell efficiency of 2E sensor at 0° angle before irradiation (left) at -5 V and after  $7 \times 10^{14}$   $n_{eq}/cm^2$  irradiation (right) at -30 V. Efficiency was 95.4% before and 91.1% after irradiation.

using source tests. Beam tests at Fermilab showed greater than 90% tracking efficiencies before irradiation and slight reduction in efficiencies of 2E and 4E sensors after irradiation. The reduced efficiencies after irradiation arise due to higher readout threshold and low electric field. Good charge collection efficiency was obtained, especially after heavy irradiation. After irradiation, 2E showed the greatest efficiency and charge collection. TCAD Simulation efforts are ongoing to understand FBK beam test results. Also, more sensors are being obtained from FBK, SINTEF and CNM. The plan is to irradiate sensors up to  $10^{16}$   $n_{eq}/cm^2$  fluence levels and obtain performance values before and after irradiation.

## References

- [1] D. Bortoletto et al., The CMS pixel system, Nucl. Instr. and Meth. A 579 (2007) 669.
- [2] The HiLumi LHC Design Study website, <http://hilumilhc.web.cern.ch/hilumilhc/index.html>
- [3] G Auzinger et al., Silicon sensor development for the CMS tracker upgrade, 2011 JINST 6 P10010.
- [4] T. Rohe et al., Radiation hardness of CMS pixel barrel modules, Nucl. Instr. and Meth. A 612 (2010) 493.
- [5] S. I. Parker et al., 3D - A proposed new architecture for solid-state radiation detector, Nucl. Instr. and Meth. A 395 (1997) 328.
- [6] Cinzia Da Via et al., 3D silicon sensors: Design, large area production and quality assurance for the ATLAS IBL pixel detector upgrade, Nucl. Instr. and Meth. A 694 (2012) 321.
- [7] M.G. Albrow et al., The FP420 R&D Project: Higgs and New Physics with forward protons at the LHC., 2009 JINST 4 T10001.
- [8] A. Zoboli et al., Double-Sided, Double-Type-Column 3-D Detectors: Design, Fabrication, and Technology Evaluation, IEEE Trans. Nucl. Sc. NS-55 (5) (2008) 2775.
- [9] G. Pellegrini et al., First double-sided 3-D detectors fabricated at CNM-IMB, Nuclear Instruments and Methods in Physics Research Section A592 (2008) 38..
- [10] L. Uplegger et al., Test-beam studies of diamond sensors for SLHC, in press, doi:10.1016/j.nima.2012.11.076
- [11] M. Obertino et al., 3D-FBK pixel sensors with CMS readout: First test results, doi:10.1016/j.nima.2012.10.011
- [12] O. Koybasi et al., Assembly and qualification procedures of CMS forward pixel detector modules, Nucl. Instr. and Meth. A 638 (2011) 55.
- [13] O. Koybasi et al., Electrical Characterization and Preliminary Beam Test Results of 3D Silicon CMS Pixel Detectors, IEEE Trans. Nucl. Sc. 58 (2011) 1315.
- [14] E. Alagoz et al., Simulation and laboratory test results of 3D CMS pixel detectors for HL-LHC, 2012, JINST 7 P08023
- [15] M. Povoli et al., Impact of the layout on the electrical characteristics of double-sided silicon 3D sensors fabricated at FBK, 2012, JINST 7 P08023
- [16] M. Povoli et al., Slim edges in double-sided silicon 3D detectors, 2012, JINST 7 C01015.
- [17] S. M. Sze, K. K. Ng, Physics of Semiconductor Devices, Wiley Inter-Science, 2006.